ISSN 0742-0463, Journal of Volcanology and Seismology, 2018, Vol. 12, No. 4, pp. 252–267. © Pleiades Publishing, Ltd., 2018.
Original Russian Text © Yu.I. Blokh, V.I. Bondarenko, A.S. Dolgal', P.N. Novikova, V.V. Petrova, O.V. Pilipenko, V.A. Rashidov, A.A. Trusov, 2018, published in Vulkanologiya i Seismologiya, 2018, No. 4, pp. 26–42.

To the memory of G.B. Udintsev, the pioneer in the study of submarine volcanoes at the Kuril island arc

The Rikord Submarine Volcanic Massif, Kuril Island Arc

Yu. I. Blokh[a, *], V. I. Bondarenko[b], A. S. Dolgal'[c], P. N. Novikova[c], V. V. Petrova[d], O. V. Pilipenko[e], V. A. Rashidov[a, **], and A. A. Trusov[f]

[a] *Institute of Volcanology and Seismology, Far East Branch, Russian Academy of Sciences, bul'var Piipa 9, Petropavlovsk-Kamchatskii, 683006 Russia*

[b] *Nekrasov State University, ul. 1 Maya, 16, Kostroma, 156961 Russia*

[c] *Mining Institute, Ural Branch, Russian Academy of Sciences, ul. Sibirskaya, 78a, Perm', 614007 Russia*

[d] *Geological Institute, Russian Academy of Sciences, Pyzhevskii per., 7, Moscow, 109017 Russia*

[e] *Shmidt Institute of Physics of the Earth, Russian Academy of Sciences, ul. B. Gruzinskaya, 10, str. 1, Moscow, 123995 Russia*

[f] *AO GNPP Aerofizika, Pokhodnyi proezd, 19, Moscow, 125373 Russia*

**e-mail: yuri_blokh@mail.ru*

***e-mail: rashidva@kscnet.ru*

Received May 15, 2017

Abstract—This paper reports a study of the Rikord volcanic massif. The massif consists of four volcanic edifices that coalesce in their bases, and is most likely Quaternary. The massif discharged basaltic and basaltic andesite lavas during its earlier life. The observed high natural remanent magnetization that was found in dredged rocks is due to high concentrations of single-domain and pseudo-single-domain grains of titanomagnetite and magnetite. We have identified the directions of the conduits and the presence of peripheral magma chambers. A 3D model has been developed for the central part of the Rikord volcanic massif; the model includes ten large disturbing magnetic blocks that are most likely cooled, nearly vertical, conduits.

DOI: 10.1134/S0742046318040024

INTRODUCTION

The Rikord submarine flat-summit volcanic massif was so named in honor of the well-known Russian navigator Petr Ivanovich Rikord, an investigator of the Russian Far East seas (Bezrukov et al., 1958). The massif lies in the central Kurils, in the middle of the eponymous strait between Ketoi and Ushishir islands (Fig. 1).

The Rikord massif was investigated during the 1949–1955 cruises launched by the Institute of Oceanology and during five cruises of the R/V *Vulkanolog* in 1982–1991 carried out by the Institute of Volcanology, Far East Branch, USSR Academy of Sciences (Bezrukov et al., 1958; *Podvodnyi vulkanizm ...,* 1992). The *Vulkanolog* survey included echo sounding, continuous seismoacoustic profiling (CSP), modular hydromagnetic surveying (HMS), and dredging over the near-summit part of the submarine volcanic massif (Anikin et al., 2017; Blokh et al., 2013, 2014, 2015, 2017; Bondarenko and Rashidov, 2007, 2011a, 2011b; *Podvodnyi vulkanizm ...,* 1992).

The present paper is a review of the surveys conducted during cruises of the R/V *Vulkanolog* and of experiments in modern geophysical laboratories using dredged rock material.

THE MORPHOSTRUCTURE

The submarine volcanoes in the central Kurils mostly align themselves in chains that trend in different directions; the volcanoes are confined to hypothetical, primarily dextral strike slip or to the anxiliary fractures around them. The strike slip separate the central Kurils into four segments with different morphostructures: Matua I. to Nadezhda Strait, Rasshua I. to Ushishir Is., Rikord Strait to Diana Strait, and the Simushir I. area (Bondarenko and Rashidov, 2011a, 2011b).

The central Kurils have experienced considerable subsidence with amplitudes ranging between a few hundreds of meters and 1 kilometer during Quaternary time.

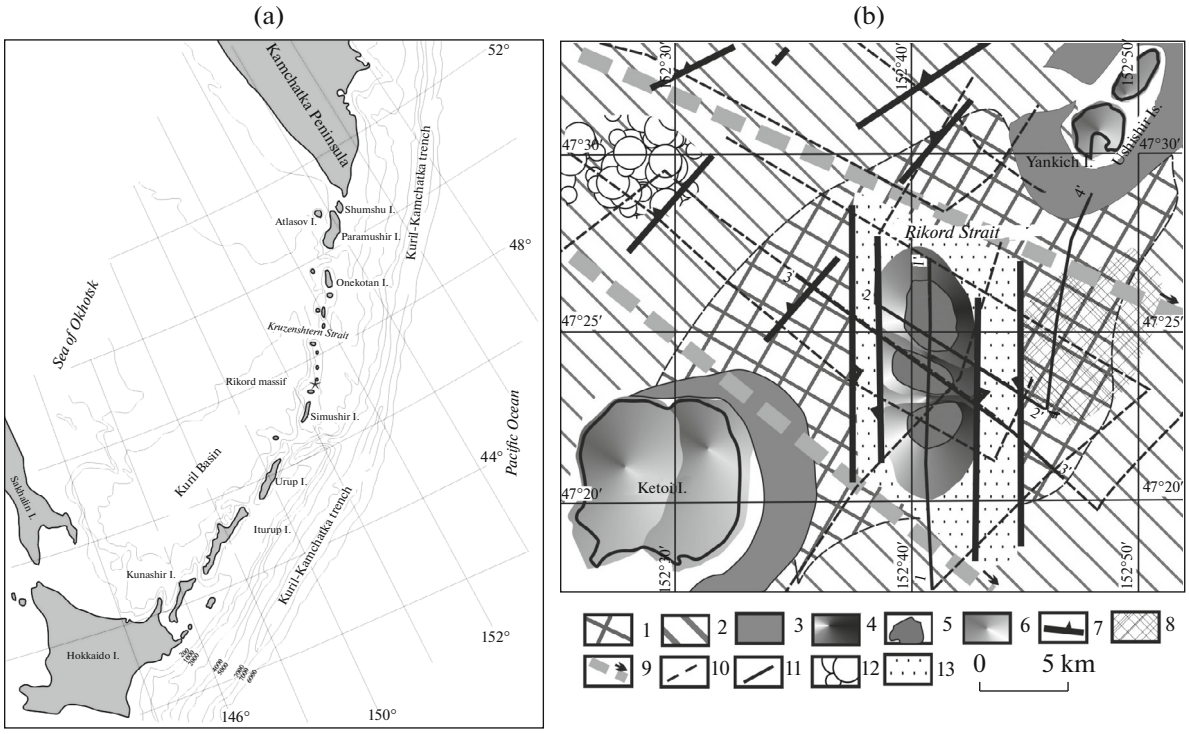

Fig. 1. The location of the Rikord submarine volcanic massif (a) and a morphostructural sketch of the Rikord Strait (b). (1) erosional and erosion–tectonic seafloor surfaces in the Kuril straits; (2) steep (>10°) erosion–tectonic or erosion–volcanogenic seafloor surfaces in the upper parts of slopes around the Greater Kuril arc; (3) flat seafloor areas at depths below 140–160 m corresponding to the Holocene sea level rise; (4) submarine volcanoes; (5) flattened summits of submarine volcanoes; (6) volcanoes on land; (7) faults identified by geophysical surveys; (8) buried older abrasion surfaces; (9) inferred zones of strike slips; (10) geophysical survey lines; (11) fragments of CSP lines, with resulting seismograms presented in Figs. 3 and 4; (12) areas of landslide deposits; (13) Rikord graben.

The base of the Rikord submarine volcanic massif is at depths of 600–700 m; its flat 2 × 9-km summit is at 130–150 m (see Figs. 1a, 1b). The base of the massif is 9 × 19 km, while the volume is approximately 50 km^3.

The northern, western, and eastern slopes of the massif are very steep, occasionally dipping at 20°–30°. The southern slopes are more gentle, at 3°–7°. The seafloor around the massif is uneven. This is probably due to intense erosional activity of currents, especially tidal currents, which can be as fast in the strait as 1.5–4 knots. The massif consists of four volcanic edifices whose bases have coalesced. The Rikord massif is separated from the Ushishir Islands by seafloor areas whose depths are 600–700 m, with the corresponding seafloor areas off Ketoi Island at depths of 350–400 m.

SEISMOACOUSTIC SURVEYS

Judging from the seismoacoustic images, the massif consists of both dense effusive rocks and unconsolidated, apparently pyroclastic and sedimentary rocks. Geophysical studies have revealed four distinct edifices whose bases have coalesced (Blokh et al., 2013, 2017); the edifices are composed of predominantly massive volcanic rocks (Fig. 3a, V.1–V.4).

The V.1, V.2, and V.4 volcanoes (see Fig. 3) have their flat summits at a depth of approximately 150 m. There are small (within 200 m) lows between these. The depths of the flat summits are at the depth of the Late Pleistocene underwater terrace that resulted from the considerable lowering of the Sea of Okhotsk during the last glaciation (Bezrukov et al., 1958; Gorshkov, 1967; *Kamchatka ...,* 1974). We are thus entitled to hypothesize that the Rikord edifices date from pre-Holocene time. CSP surveying revealed between V.1 and V.2 a peculiar rock sequence of variably alternating deposits that are characterized by numerous, long, dipping intensive reflectors (see Fig. 3a). These are 0.25–0.3 s thick in the scale of the two wave travel time (TWT), which can amount to 250–300 m on the assumption of 2000 m/s for the speed of sound. The character of the seismoacoustic image of the section suggests V.1 and V.2 as the source of material for this rock sequence, with the transport occurring simultaneously from both volcanoes. The deposits were probably formed during Late Pleistocene time, resulting from redeposition of the material that came from truncation of the summits. Volcano V.3 is at present com-

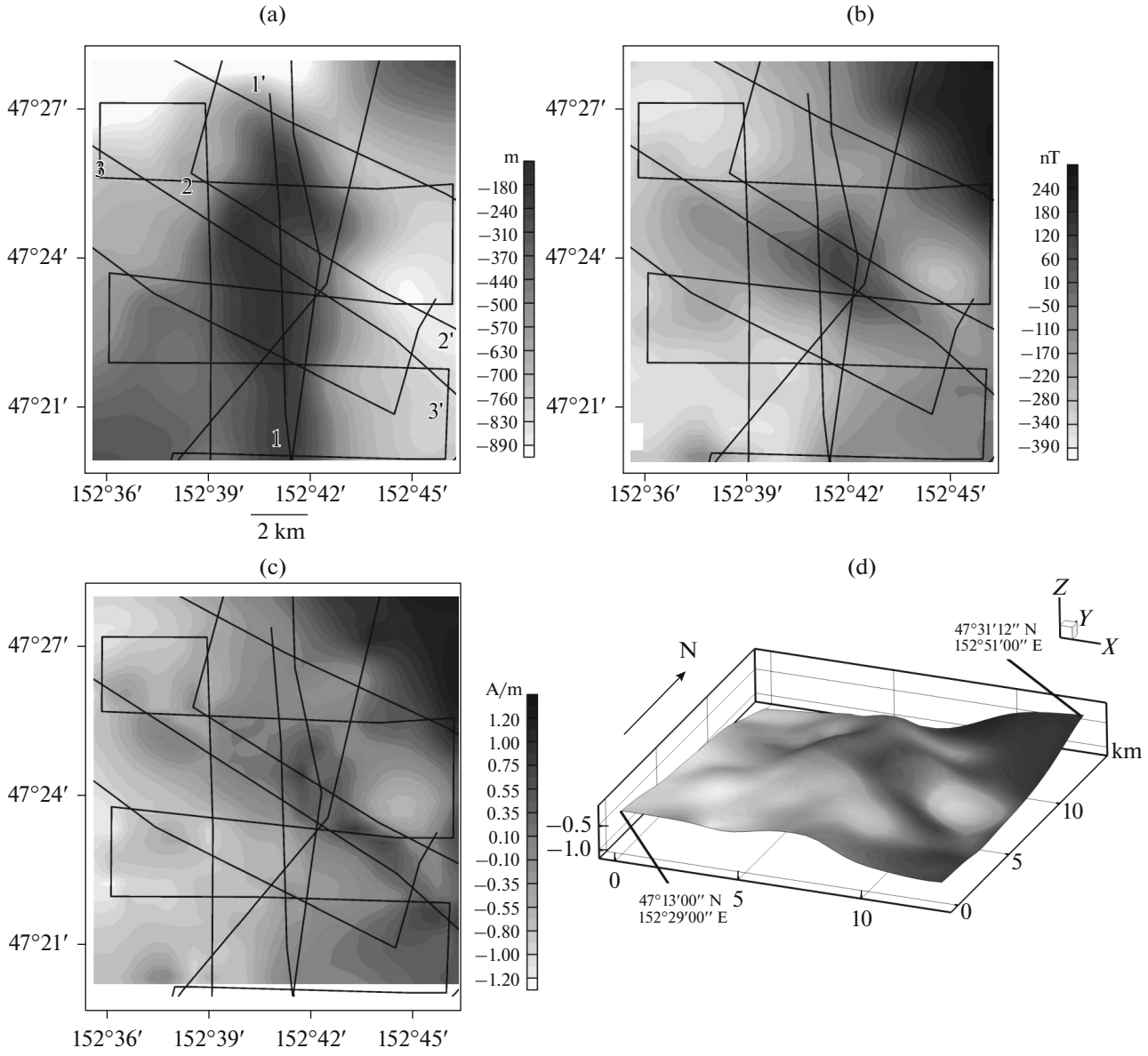

Fig. 2. The Rikord submarine volcanic massif. (a) bathymetry; (b) anomalous magnetic field ΔT_a; (c) distribution of effective magnetization J_{ef} on the volcano; (d) distribution of effective magnetization J_{ef} as shown on the volcano's surface. Numerals mark the lines shown in Figs. 1b, 3, and 9.

pletely buried under sediments and its summit is at depths of 230–250 m.

The southern, relatively less steep, slopes of the massif were found to clearly show clinoforms of lateral accretion with tangential cross-bedding (see Fig. 3a). This unit has a total thickness of 0.3-s TWT in the upper part to 0.2-s TWT at the base of the massif. The observed picture provides evidence of a high-energy sedimentation setting that involved intensive inflow of unconsolidated material, as well as indicating Volcano V. 4 as the main source of the material. Most likely, the material came from erosion of the Rikord summit during Late Pleistocene time.

A number of faults are clearly identified in the Rikord Strait based on CSP data (see Figs. 1b, 3). The features in the seismoacoustic image of the section, the pattern of the faults identified in the area, and the relative positions of summit surfaces at the Great Kuril island arc in the Rasshua–Ushishir area and in the area between the Rikord massif and Simushir Island, all suggest the presence of major fault zones at the boundaries of these areas (see Fig. 3) involving strike-slip movements (probably a right lateral strike-slip fault and a normal-oblique fault) between the Ushishir Islands and the Rikord submarine volcanic massif, as well as in the southern part of the strait, between the

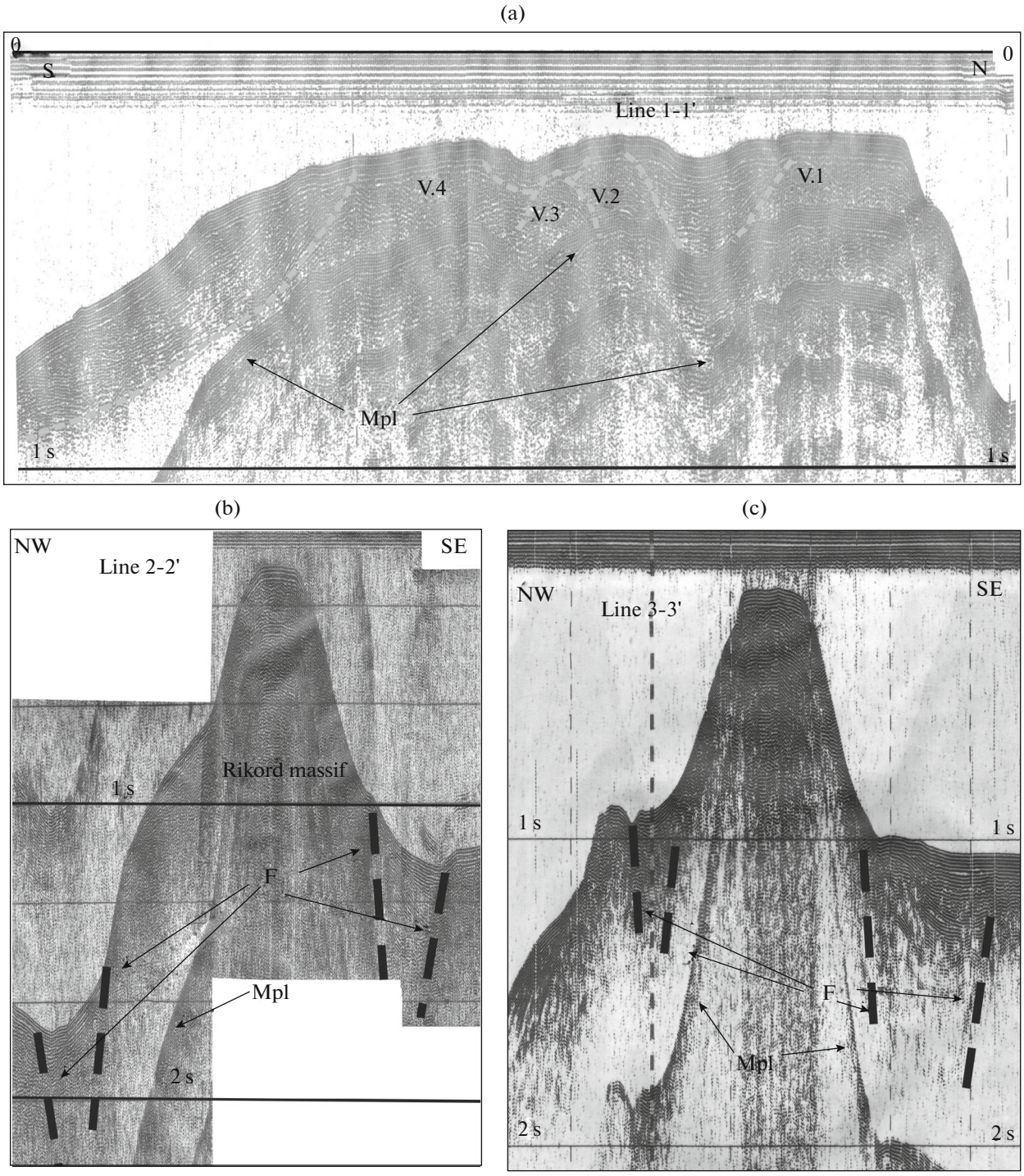

Fig. 3. Fragments of CSP seismogram as recorded on lines 1–3. Mpl, multiple reflections; F, faults; V.1, V.2 ... the volcanic edifices that make up the Rikord massif. The spatial locations of the lines can be seen in Fig. 1b.

Rikord massif and Ketoi Island (Bondarenko and Rashidov, 2007). The Rikord massif itself lies within the nearly north–south graben-like structure that we have called the Rikord graben. The formation of the graben may have been related to strike-slip movements on the strike-slip zones mentioned above following the mechanism of pull-apart depressions (Prokop'ev et al., 2004; Tevelev and Tevelev, 1996). The crustal extension that accompanies the formation of the Rikord graben may have resulted in resumption of magmatism and in the origination of the submarine volcanic massif.

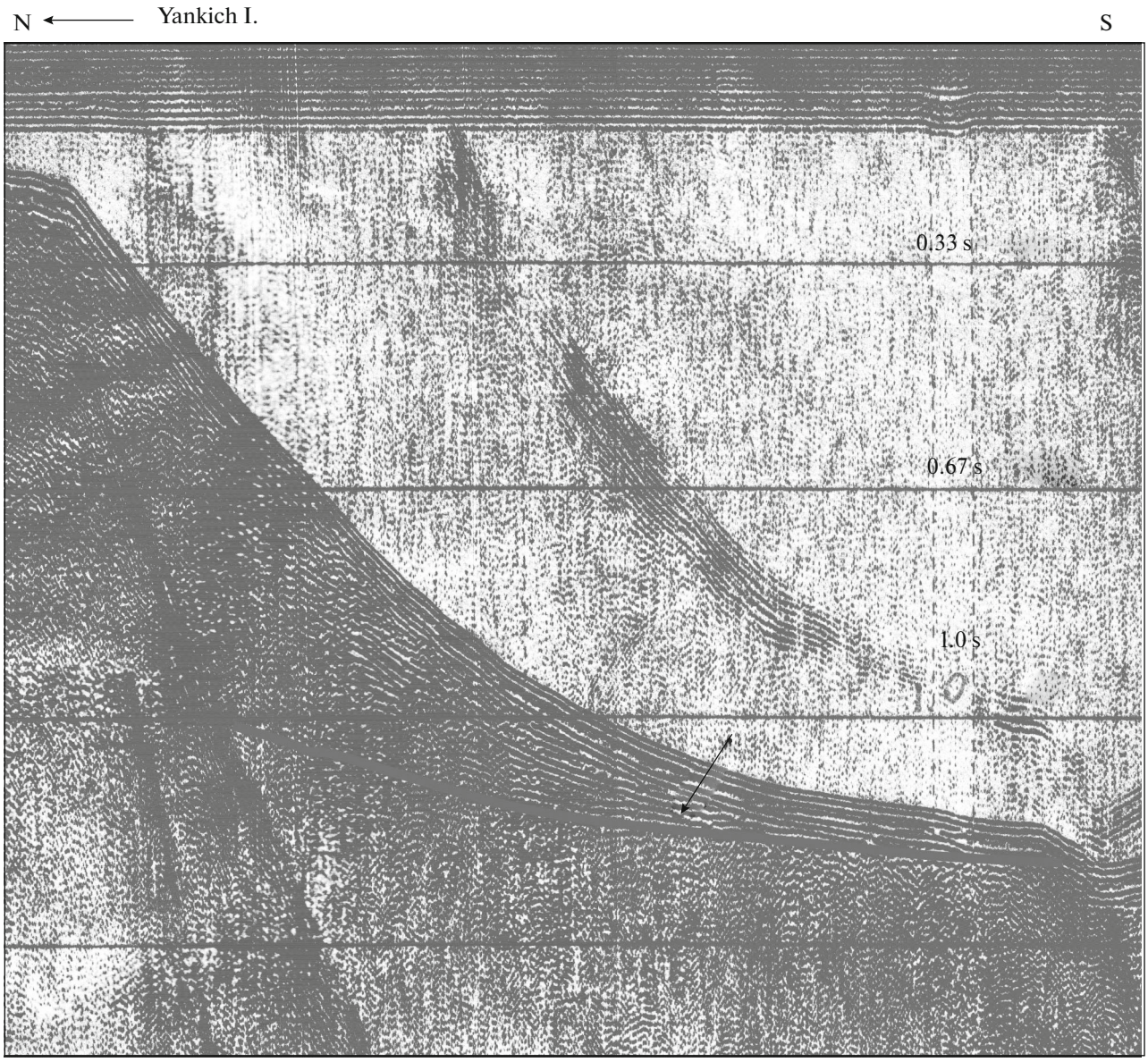

Fig. 4. A fragment of a CSP seismogram along line 4. The arrow indicates a low-angle reflector. The location of the line is shown in Fig. 1b.

A gently dipping reflecting interface on the CSP sections occurs east of the Rikord massif at depths of 800–900 m (Fig. 4). Below that interface, we find nearly no regular reflections on the CSP seismograms upon a rather high level of recorded irregular signals. This reflector seems to be an older abrasion peneplain that was formed in volcanic rocks.

In the northern direction, this surface is overlain by the lower part of the Ushishir volcanic massif, which is most likely composed of predominantly unconsolidated deposits (Bondarenko and Rashidov, 2007). The deposits become rapidly thicker toward Yankich Island (see Fig. 4). The long reflectors that are clearly seen in the CSP seismograms within this rock sequence make a fan that diverges toward the island. The observed picture indicates that the incoming material that composed the rock sequence was not regular in its supply and that the source of the material was in the Ushishir Islands area. The active Ushishir Volcano was most likely the source. It is generally thought (Bondarenko, 1986, 2015; Gorshkov, 1967; *Kamchatka ...,* 1974) that the Ushishir massif dates back to the Quaternary. The surface that its base overlies is older, Early Quaternary or Late Pliocene. Its present-day location at a depth of 800–900 m indicates a considerable Quaternary subsidence of the area by approximately 900 m.

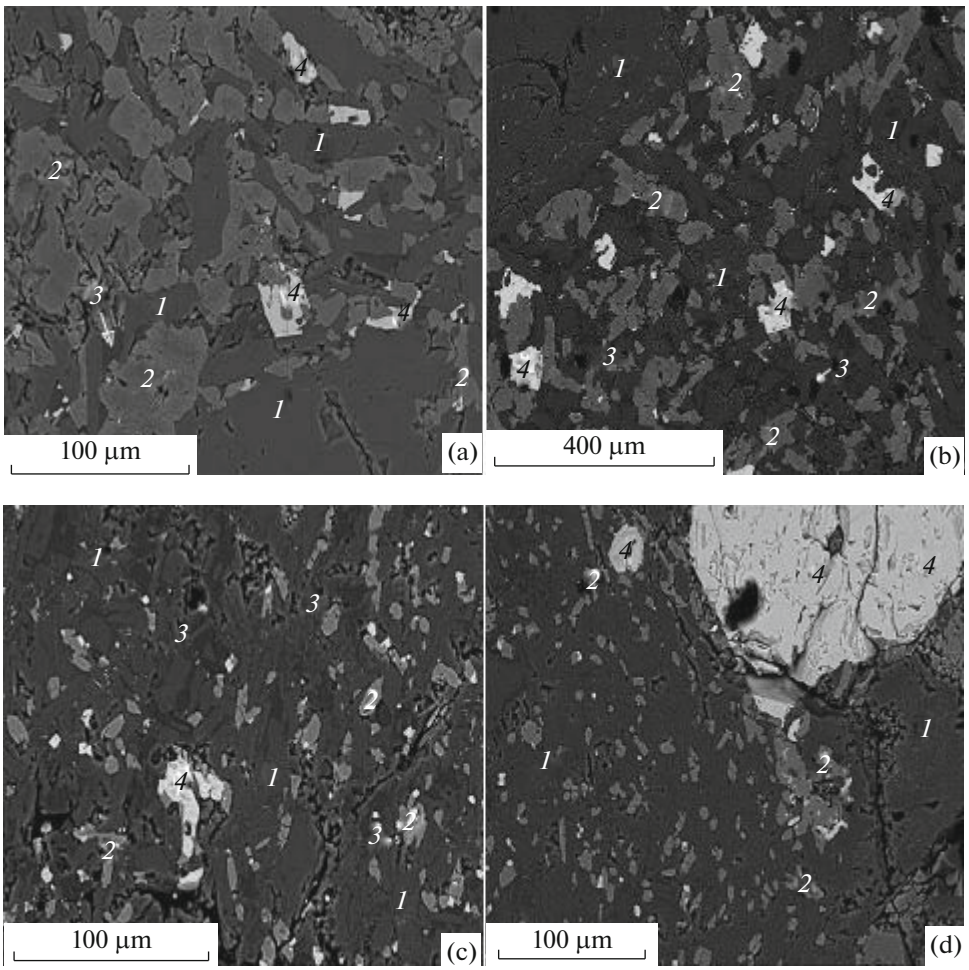

Fig. 5. Basalt textures in sample B25-32/3 (a, b) and andesite textures in sample B25-32/9 (c, d). (*1*) plagioclase; (*2*) monoclinic pyroxene; (*3*) volcanic glass or quartz; (*4*) titanomagnetite.

The surface of the unconformity is bounded on the west by the Rikord graben. The Rikord graben and massif are younger than this abrasion surface, that is, Quaternary (possibly Middle to Late Pleistocene).

PETROGRAPHIC STUDIES

A segment approximately 1 km long was dredged at depths of 360–270 m within the near-summit part of the volcanic massif during the 25th cruise of the R/V *Vulkanolog*. Various rocks were lifted, which were mostly fresh angular fragments (Blokh et al., 2013, 2017; *Podvodnyi vulkanizm ...,* 1992). The chemical compositions of the dredged rocks consist of two series: a relatively low-silica, low-potassium, high-calcium basaltic series (in wt %: SiO_2 = 48–50, K_2O = 0.1–0.3, CaO = 10.5–11.5) and a less abundant moderate- and high-silica, moderate-potassium and low-carbonate andesitic series (SiO_2 = 55–61, K_2O = 0.7–1.0, CaO = 6.5–8.5) (*Podvodnyi vulkanizm ...,* 1992). Rocks of an intermediate basaltic andesite composition are rare. Table 1 presents a short description of rocks in all the three series, while Fig. 5 shows their textures and mineral compositions.

One prominent feature in the mineralogy of the rocks that compose the near-summit part of the Rikord massif consists in the fact that a rare kind of pyroxene was found in them, viz., pigeonite. The chemical composition of the andesites clearly reveals three pyroxene varieties: augite (Ca ~ 38 mol %), pigeonite (Ca ~ 11 mol %), and hypersthene (Ca ~ 2–4 mol %). The basalts and basaltic andesites were found to have transitional compositions between clinopyroxene (pigeonite) and orthopyroxene (ferrohypersthene and hypersthene). Pigeonite cannot survive in lava as an independent mineral, unless the rock cools very rapidly, with the pigeonite composition persisting and being consistent with the initial equilibrium conditions during the eruption (Deer et al., 1962). It thus appears that the combined presence (paragenetic association) of olivine, pigeonite, and orthopyroxene can be used to assess the temperature

Table 1. The mineral composition and texture of the rocks that were dredged from the near-summit part of the Rikord submarine volcanic massif

Rock properties			Basalt	Basaltic andesite	Andesite
Texture		Of rock	Magnophyric		
		Of groundmass	Diabase, rarely trachytic	Microdoleritic, occasionally weakly trachytic, rarely hyalopilitic or interstitial	Doleritic, occasionally weakly trachytic
Phenocrysts to groundmass ratio			From 3/5 to 1/1	From 3/5 to 1/3	From 1/3 to 1\5
Phenocryst composition, %			Plagioclase (60–70), monoclinic pyroxene (10–25), olivine (1–10), rhombic pyroxene (0–3), titanomagnetite (0)	Plagioclase (70–80), monoclinic pyroxene (7–15), olivine (1–5, occasionally 10), rhombic pyroxene (0–3), titanomagnetite (<1)	Plagioclase (85–99), monoclinic pyroxene (1–15), rhombic pyroxene (0–5), olivine (0–1), titanomagnetite (0–5)
Composition of microlites, %			Plagioclase (20–50), monoclinic pyroxene (20–40) titanomagnetite (20–40), occasionally volcanic glass and quartz in interstitions	Pyroxene (~40), titanomagnetite (~40), plagioclase 20	Plagioclase (30–35), pyroxene (30–35) titanomagnetite (30–40), occasional quartz and interstitial glass
Microlite size, mm			0.01–0.1	0.01–0.1	0.01–0.1
Phenocrysts					
Plagioclase	Size (mm)		0.2–4	0.1–0.2 to 4	0.2–4.0
	Zonality		2–4	2–6	to 4
	Composition		From bitownite 89 at the center to labradorite 52 at edges	From bitownite to labradorite	From bitownite 85 at the center to andesine 38–45 at edges
	Replacement		Leaching of central zones, glassy fringes in growth zones	Twinned, rich in glass inclusions	Twinned, strongly fragmented with minute cracks, rich in inclusions of glass and occasional crystallized groundmass
	Growths		Among plagioclases, with rhombic pyroxene, and glass	Some inner zones are rich in glass inclusions (up to 90%)	With glass
Olivine	Size		0.2–0.8, occasionally 1.5	Usually below 0.1, occasionally 0.2–0.8 to 1.5	0.2–0.8
	Composition, mol %		Fo from 64.8 to 74.4, or Fa from 35.2 to 25.6	Fo 60–70	Fo 60–70
	Replacement		With iddingsite and bowlingite along cracks and edges of crystals	Weakly altered	Almost completely leached
	Growths		With rhombic and monoclinic pyroxene, titanomagnetite inclusions	With titanomagnetite	With titanomagnetite

Table 1. (Contd.)

Rock properties		Basalt	Basaltic andesite	Andesite
Monoclinic pyroxene	Size, mm	0.2–2.5	0.1–4	0.2–0.8
	Composition, mol %	Mg – from 40 to 50, Ca from 29 to 41, Fe from 18 to 24, i.e., augite and, more rarely, ferroaugite	Augite	Mg 42.8, Ca 38.1, Fe 19.1 augite Mg 44.1; Ca 11.3; Fe 44.6 pigeonite
	Replacement	Unaltered	Unaltered	Partly leached
Pigeonite	Growths	With plagioclase, olivine, and rhombic pyroxene.	With plagioclase and titanomagnetite	
Pigeonite	Size, mm	≤0.4		
Rhombic pyroxene	Composition, mol %	Mg from 44 to 68, Fe from 21 to 45, Ca from 2.6 to 12, i.e, from ferrihypersthene to hypersthene and pigeonite without breaks	Hypersthene, pigeonite	Mg 64.6; Ca 3.5; Fe 31.8 hypersthene. Compositional breaks between hypersthene and pigeonite
	Replacement	Unaltered	Unaltered	Unaltered
	Growths	Between itself, monoclinic pyroxene, olivine, and plagioclase	With olivine and plagioclase	With plagioclase
Titanomagnetite	Size	Microlites only	0.1–1.0	0.2–0.8
	Amount of FeII	0.65–0.68 formula units	0.69–0.72	0.72–0.74
	Amount of FeIII	1.44–1.49	1.58–1.63	1.53–1.59
	Amount of Ti	0.36–0.44	0.23–0.28	0.27–0.31
Interstitial glass	Chemical composition	Not encountered	Not encountered	SiO_2 = 72.32 from 81.9; TiO_2 = 0.5–1.12; Al_2O_3 = 11.8–12.22; FeO = 0.7–2.67; CaO = 2.76–3.2; Na_2O = 3.15–3.56; K_2O = 0.5–3.64

of the melt in the magma chamber as 1200–1300°C (the temperature that is suitable for the crystallization and stable existence of pigeonite).

The existence of a nearly continuous chemical series ranging from basalt to andesite, the presence of transitional varieties from andesine to bytownite to zonal plagioclase crystals, and the gradual replacement of mafic mineral associations with sialic associations all point to a genetic affinity of the dredged samples. This factual material suggests the discharge of basaltic and basaltic andesite lavas during the initial stages in the life of the Rikord volcanic massif.

As basalt was crystallizing, the parent melt was depleted in mafic components and enriched in sialic components. The differentiation resulted in the discharge of various andesite flows that showed a variable and gradually diminishing concentration of mafic minerals and an increasing concentration of plagioclase. One is then confronted with a situation in which the composition of plagioclase phenocrysts in andesites is not much more acidic than that in basalts. This probably stems from the fact that a rapidly diminishing concentration of pyroxene leads to enrichment in calcium.

It can be hypothesized that the oldest edifices in the Rikord massif are basaltic and basaltic andesite in composition, while the youngest ones are andesitic.

MAGNETIC STUDIES

The first magnetic studies showed that basalts had the highest magnetization among all dredged rocks; the natural remanent magnetization of the basalt J_n reached 10 A/m, while those showing the least magnetization were andesites, with J_n being below or equal to 0.6 A/m (Blokh et al., 2013).

The present paper reports a comprehensive magnetic study of eight samples in order to identify the main J_n carrier in the rocks that compose the Rikord volcanic massif using a previously reported technique (Rashidov et al., 2014, 2015, 2016). Cubes with 1-cm edges were used for the measurements.

The J_n in the samples was measured using a JR-6 magnetometer (AGICO, Czech Republic) in three orthogonal positions of a rotated sample. The magnetic susceptibility, æ, and the degree of anisotropy in the magnetic susceptibility, P', were determined using a Multi-Function Kappabridge kappameter (AGICO, Czech Republic).

For each sample we measured magnetic hysteresis curves (Fig. 6) using a vibrating-sample magnetometer (ORION, Russia) with subsequent measurement of the domain state based on the J_{rs}/J_s and B_{cr}/B_c ratios (Day et al., 1977) (Fig. 7a). The magnetic parameters based on the magnetic hysteresis curves (Table 2) were found after correcting for the paramagnetic background value (Jp).

The composition of the ferromagnetic fraction was studied by thermomagnetic analysis (TMA) based on the relationship between remanent saturation magnetization J_{rs} and temperature T using a two-component thermal magnetometer (ORION, Russia) in ambient air.

These magnetic studies of basalt samples (samples B25-32/3, B25-32/4, B25-32/5, B25-32/11, and B25-32/12) and basaltic andesite sample B25-32/1 showed that the high values of $J_n = 2–9$ A/m were due to high concentrations (æ = (9–23) × 10^{-3} SI) of single-domain and pseudo-single-domain grains (SD-PSD) in low-coercive (B_{cr} = 18–23 mT) ferromagnetic minerals. The samples had a low degree of magnetic anisotropy (see Table 2).

The relatively low values of J_n = 0.2–0.9 A/m in basaltic andesite (sample B25-32/16) and in andesite (sample B25-32/9) are due to a high concentration (æ = (15–33) × 10^{-3} SI) of pseudo-single-domain and multidomain grains (PSD-MD) in low-coercive (B_{cr} = 12–23 mT) ferromagnetic minerals. These samples also show low degrees of magnetic anisotropy (see Table 2).

All rock samples investigated here can also be subdivided into two sets based on the behavior of the curves of thermomagnetic analysis $J_{rs}(T)$.

One set includes samples of basalt (samples B25-32/3, B25-32/4, B25-32/11, B25-32/12) and basaltic andesite (samples B25-32/1, B25-32/16). TMA showed that

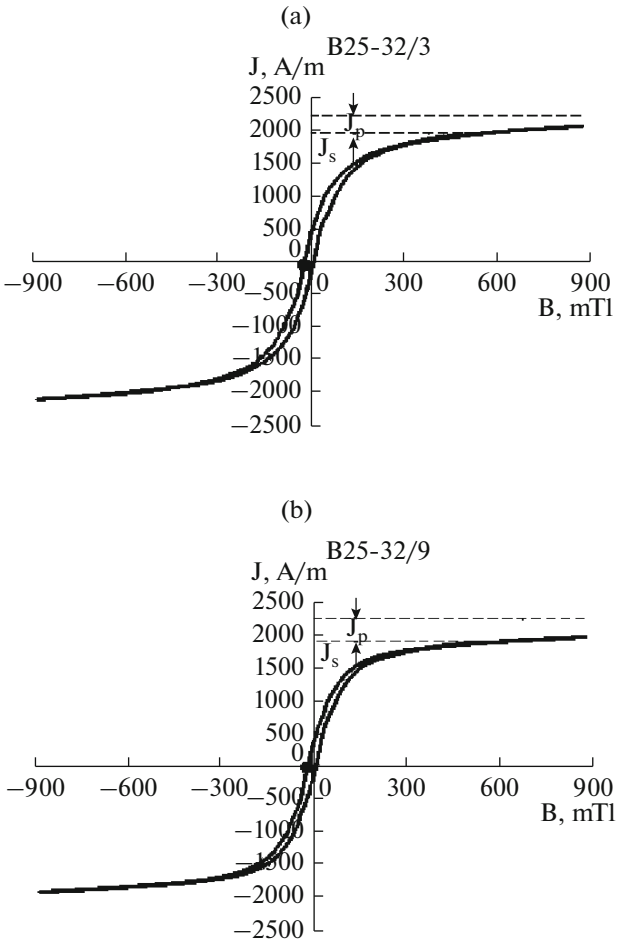

Fig. 6. Sample curves of magnetic hysteresis in samples where the main carriers of magnetization are magnetite (a) and titanomaghemite (b). J_p is the petromagnetic contribution into magnetization; J_s is saturation magnetization.

the first-heating curves had their inflexion points in the interval ~490–575°C (see Fig. 7b). The second-heating curves are higher, irreversible, and have an inflexion point at ~575°C. The main carrier of magnetization in these samples is a low-Ti titanomagnetite whose composition is similar to that of magnetite. The high Curie points are due to a likely high-temperature oxidation affecting titanomagnetite when still in situ conditions, resulting in decomposition into a phase similar to magnetite and hemo-ilmenite. The growth in magnetization on heating to 600°C and subsequent cooling is due to further heterophase decomposition of titanomagnetite.

The amount of Ti deduced from a microprobe analysis of microlites and phenocrysts in basaltic samples B25-32/3 and B25-32/11 and in basaltic andesite sample B25-32/16 yielded much lower Curie points, indicating the presence of titanomaghemite. This is another piece of evidence to corroborate the invariable presence of several ferrimagnetic phases in actual oceanic basalts, including titanomaghemite, as well as

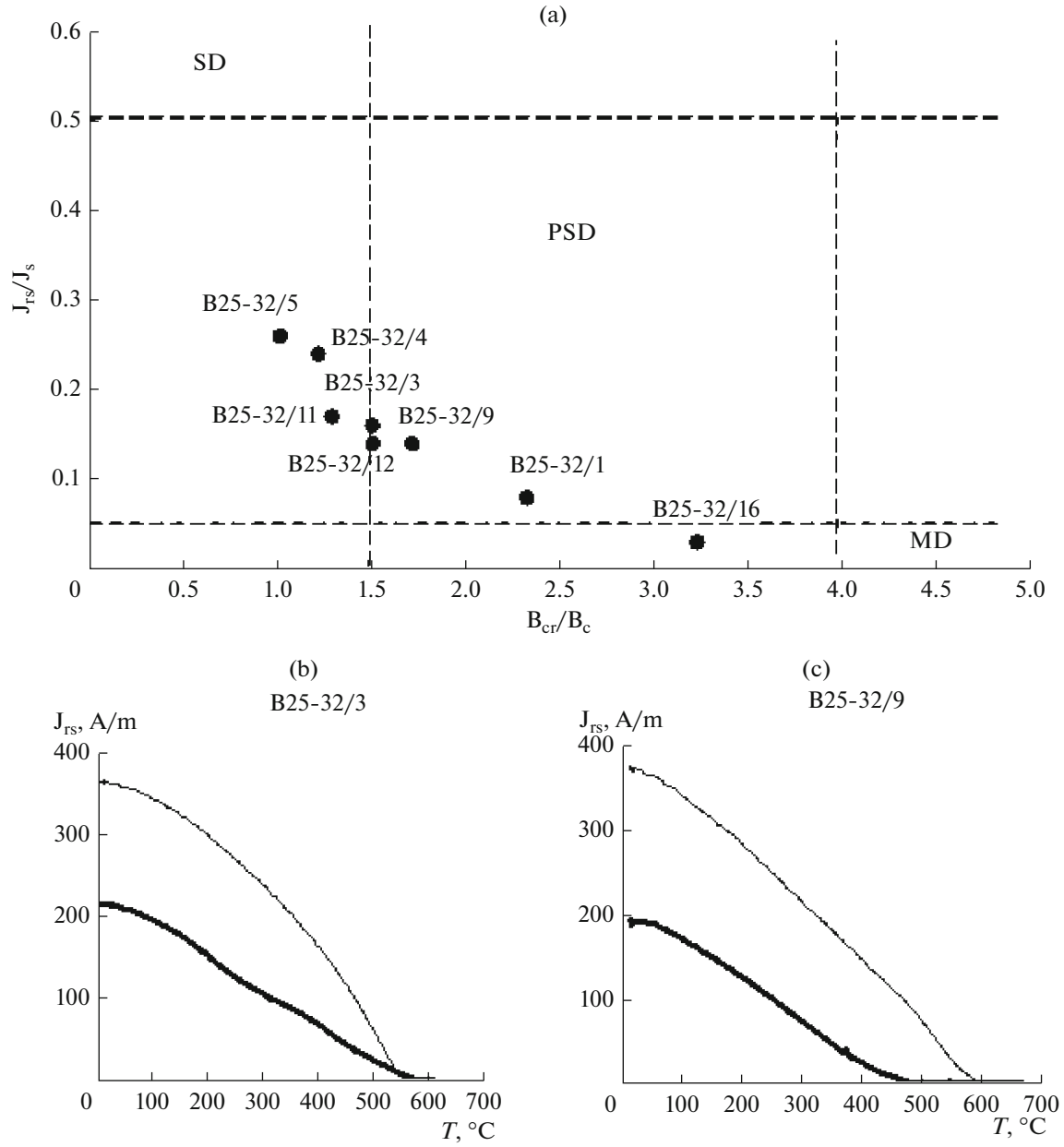

Fig. 7. A Day diagram (a) and curves of thermomagnetic analysis $J_{rs}(T)$ for samples where the main carrier of magnetization is magnetite (b) and titanomaghemite (c).

products of its single-phase and/or heterophase oxidation (*Priroda ...,* 1996).

The other set identified from the behavior of TMA curves includes basalt (sample B25-32/5) and andesite (sample B25-32/9). The curve of the first heating has an inflexion point around ~380–420° (see Fig. 7c). The curve of the second heating is also much higher, is irreversible, and has an inflexion point at ~575°C. The main carrier of magnetization in these samples might be titanomagnetite with concentrations of Ti X ~ 0.22–0.28 or titanomaghemite. The growth of magnetization on heating to 600°C and subsequent cooling is due to the heterophase decomposition of titanomagnetite (or titanomaghemite).

A microprobe analysis showed that the microlites in andesite sample B25-32/9 (see Figs. 5c, d) have concentrations of Ti (X ~ 0.27–0.31) corresponding to the theoretical Curie points of ~350–380°C, which is somewhat below the experimental values. The main magnetization carrier in this sample is a single-phase-oxidized titanomagnetite. This is in keeping with the result from the chemical analysis of titanomagnetite, viz., that the titanomagnetite has possibly been oxidized.

Table 2. The petromagnetic characteristics of the rocks that make up the Rikord underwater volcanic massif

No.	Samples	Rock	J_n, A/m	æ, 10^{-3}, SI	Q_n	P'	$B_{0.5}$, mT	J_{rs}, A/m	J_s, A/m	J_{rs}/J_s	B_{cr}, mT	B_c, mT	B_{cr}/B_c	Texture	C, %
1	B25-32/1-1	Basaltic andesite	2.35	17.88	3.30	1.030	–	175.0	2120	0.08	18	7.70	2.34	PSD	0.47
2	B25-32/1-2		2.74				49								
3	B25-32/3-1	Basalt	3.96	11.81	8.42	1.032	–	301.6	1890	0.16	22	14.50	1.52	PSD	0.42
4	B25-32/3-2		3.50				29								
5	B25-32/4-1	Basalt	3.51	12.51	7.05	1.058	–	518.3	2175	0.24	22	17.88	1.23	PSD, SD	0.45
6	B25-32/4-2		3.41				29								
7	B25-32/5-1	Basalt	5.99	9.07	16.60	1.056	–	413.3	1620	0.26	18	17.50	1.03	PSD, SD	0.45
8	B25-32/5-2		5.86				55								
9	B25-32/9-1	Andesite	0.87	14.57	1.50	1.036	–	259.6	1800	0.14	23	13.30	1.73	PSD	0.47
10	B25-32/9-2		0.65				97								
11	B25-32/11-1	Basalt	5.32	13.67	9.78	1.024	–	449.1	2650	0.17	23	17.65	1.30	PSD, SD	0.55
12	B25-32/11-2		5.25				28								
13	B25-32/12-1	Plagio-basalt	8.57	22.94	9.39	1.021		567.7	3950	0.14	19	12.50	1.52	PSD	0.84
14	B25-32/12-2		7.80				80								
15	B25-32/16-1	Andesite	0.21	33.47	0.16	1.009	–	114.0	3475	0.03	12	3.70	3.24	PSD, MD	0.78
16	B25-32/16-2		0.14												

J_n, natural remanent magnetization; æ, magnetic susceptibility; Q_n, Koenigsberger ratio; P', degree of anisotropy in magnetic susceptibility; $B_{0.5}$, median field; J_{rs}, remanent saturation magnetization; J_s, saturation magnetization; B_{cr}, remanent coercive force; B_c, coercive force; MD, multidomain grains; PSD, pseudo-single-domain grains; SD, single-domain grains; C, volumetric concentration of ferrimagnetic material.

Basalt dredging usually yields samples from the edges of a lava flow (*Priroda ...,* 1996). Crystallization was occurring rather rapidly in the outer parts of a lava flow. They typically show single-domain and pseudo-single-domain textures of ferrimagnetic grains. The presence of pigeonite provides evidence of very rapid cooling. Titanomagnetite phenocrysts in olivine crystals provide evidence of titanomagnetite crystallization occurring during the earlier stages in the formation of the rock.

The Koenigsberger ratio lies in the range between 1.5 and 16.6 for all basalt samples, that is, considerably above unity. This supports the hypothesis that these basalts are the chief source of the observed magnetic anomalies due to the Rikord submarine volcanic massif.

GEOMAGNETIC SURVEYS

The anomalous magnetic field ΔT_a of the Rikord submarine volcanic massif exhibits a complicated mosaic pattern that provides indirect evidence of its origin as several volcanic cones that have coalesced. The magnetic anomalies within the massif have intensities in the range (–500...+1000) nT (see Fig. 2b).

The present interpretation of the geomagnetic data was based on our own technology of MHS data simulation in combination with echo sounding, CSP, and the analysis of natural remanent magnetization J_n and the chemical composition of dredged rocks (Blokh et al., 2012). We used various interpretation methods; some of these are aimed at the 2D and 2.5D analysis of magnetic fields along individual tacks, while others involved the entire data set. Our calculations were based on the true topography of volcanic edifices, taking the basement buried under sediments into account as revealed by echo sounding and CSP. More accurate results for the deeper structure of submarine volcanoes were obtained using the method of singular points, interpretation tomography, and the fitting method for dealing with magnetic inversion problems (MIPs).

We used the IGLA software (Blokh et al., 2015, 2017; Blokh and Trusov, 2007) to determine that the vector of effective magnetization deviated from the normal field vector $\mathbf{T_0}$ toward the southwest by an angle of approximately 80°. The software implements linear inversion in a multangular interpretation window by adjusting the model in interactive mode in the shape of a truncated pyramid. Figure 8 shows the initial sites where the magnetic field was measured and the fitted model; as well, it shows the distribution of bedrock magnetization obtained using the REIST software.

This direction of the magnetization vector is rather typical of rocks in submarine volcanoes in the middle of the Kuril island arc, while its variation within the region provides evidence of periods of geomagnetic

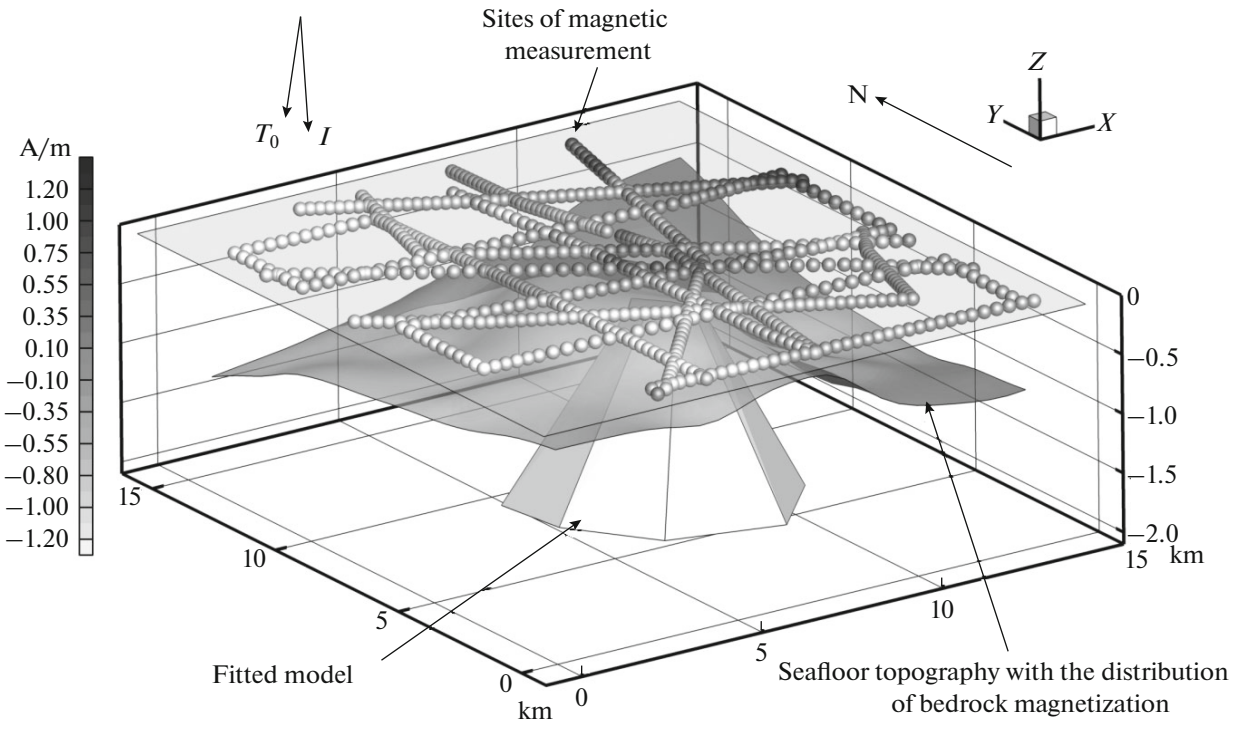

Fig. 8. Refining the direction of the magnetization vector in the Rikord submarine volcanic massif using IGLA software.

inversions coinciding with the times when the submarine volcanoes were born (Blokh et al., 2015). The available determinations of absolute age for volcanic rocks sampled in the central Kuril Islands vary in the range between 620 ka and 3.3 Ma (Lelikov and Emel'yaova, 2007; Ishizuka et al., 2011). It should be emphasized that the age of a sample taken by Japanese researchers on the Ushishir Islands, near the submarine volcanic massif under study here, is 1.17 Ma (Ishizuka et al., 2011). It can therefore be surmised that the Rikord volcanic massif was formed during the last Matuyama–Brunhes geomagnetic inversion.

The singular points of functions that describe anomalous fields for individual tacks were analyzed using the SINGULAR integrated system (Blokh et al., 1993), which implemented the well-known methods due to V.N. Strakhov, V.M. Berezkin, and G.A. Troshkov. The results showed that the main features of the functions that describe anomalous fields were confined to the top of the volcanic rocks (Fig. 9) and supported the existence of four volcanic edifices as identified by CSP.

Apart from this, the vertical distributions of localized singular points suggested a nearly vertical, a southwestern, and a south-southeastern direction of the conduits and the presence of peripheral magma chambers at a depth of ~2 km.

Three-dimensional simulation of the volcanic edifice using the REIST software from the SIGMA-3D gravity and magnetic interpretation program package (Babayants et al., 2004, 2005) showed that the maximum effective magnetization in the Rikord massif reaches 0.7 A/m (see Figs. 2c, d). The rms error achieved by 70 iterations in fitting the anomalous magnetic field was 30 nT.

The tomographic analysis of the Rikord submarine massif revealed a mosaic character of the associated anomalous magnetic field (Blokh et al., 2013). The leading tendency in the distribution of effective magnetization consists in several local zones coalescing with increasing depth. One especially notices two positive anomalous zones of J_{ef} in the central and southwestern parts of the massif that extend as far down as 5–6 km.

The mixed MIP was solved by the fitting method, resulting in a 3D model of the central part of the volcanic massif and identifying ten major magnetically disturbing blocks (Fig. 10, Table 3) whose effective magnetizations vary in the range between 1 and 2 A/m; these blocks are hypothesized to be cooled conduits. It is worth noting that several geologic features in close proximity produce most of the magnetic anomalies.

The blocks can be roughly subdivided into two sets by the direction of the magnetization vector: those whose deviation from the vertical is between 2° and 11° and those with 14° to 23°; we believe that they trend SW and SSE, which is quite consistent with the analysis of the magnetic field using the IGLA software. This

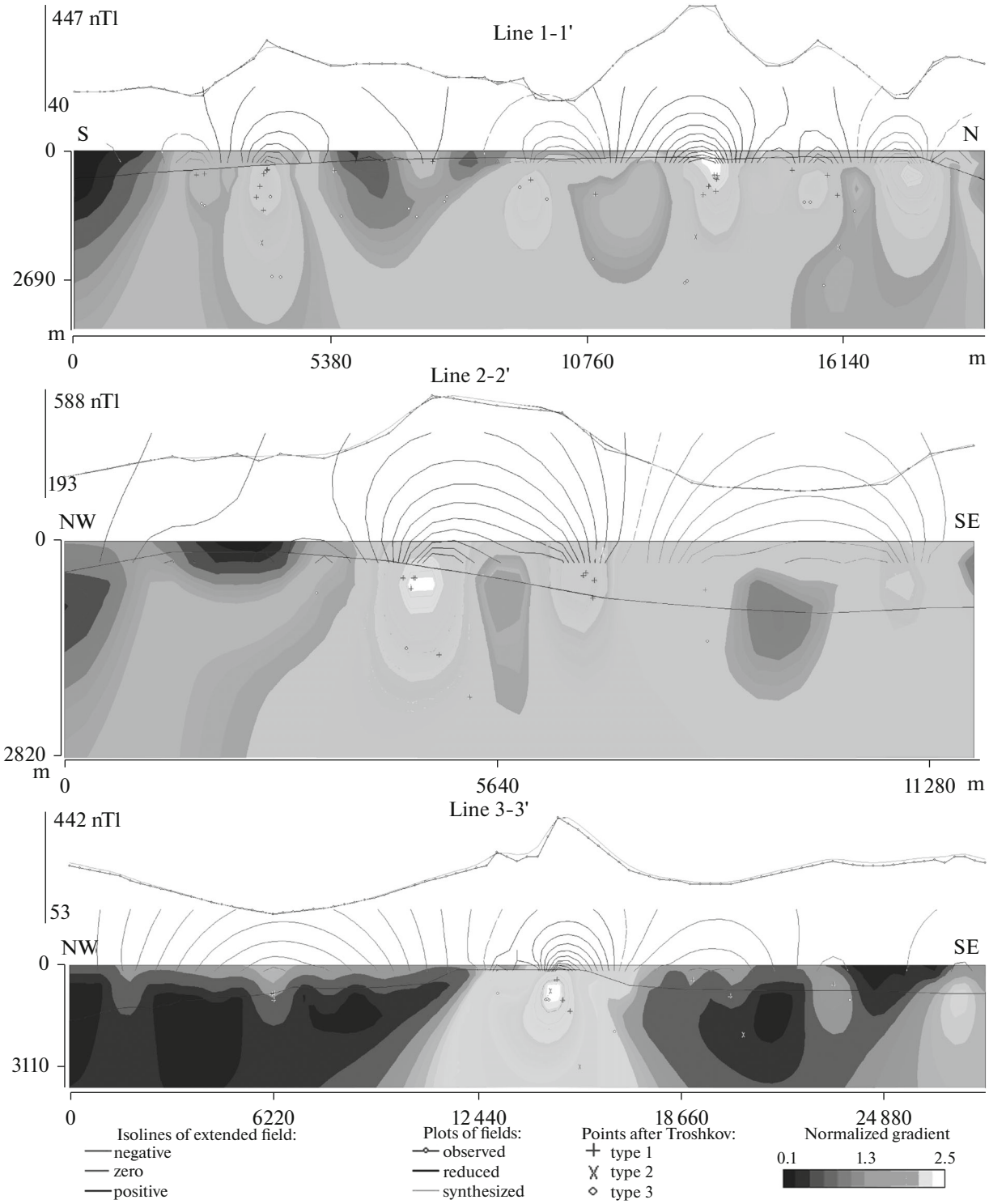

Fig. 9. An image synthesized by the SINGULAR software for location of singular points in a function that describes the anomalous magnetic field ΔT_a in the Rikord submarine volcanic massif; it is superposed on seafloor topography. The locations of the lines are shown in Figs. 1b and 2.

may indicate a consistent timing of the formation of these disturbing blocks and periods of magnetic inversion when the Earth's magnetizing field was rapidly changing in direction.

The depths to the tops of most features identified here are in agreement with the topography of the volcanic massif, with the features themselves reaching depths of 5.4 to 10 km below sea level.

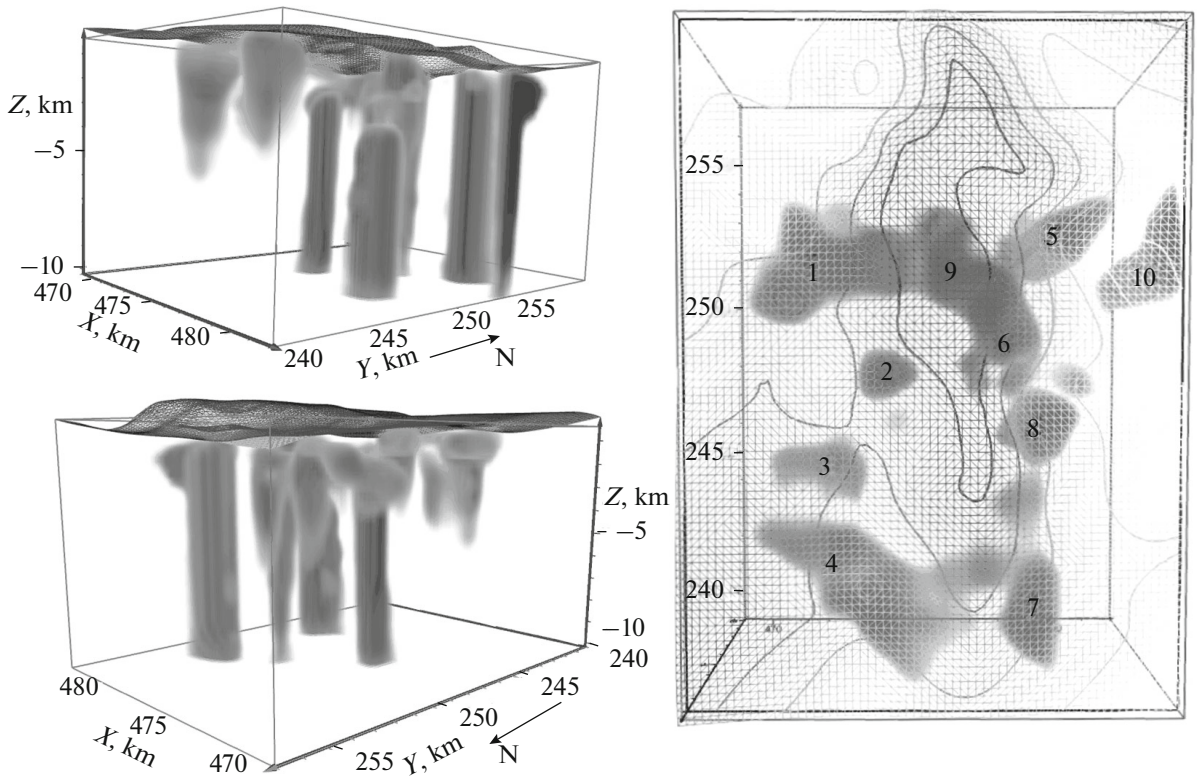

Fig. 10. A 3-D geomagnetic model for the central part of the Rikord submarine volcanic massif. Numerals mark major magnetically disturbing blocks whose values of effective magnetization J_{ef} are listed in Table 3.

Comparison between the results of geomagnetic simulation and the data supplied by petrologic and magnetic studies of rocks suggests that the Rikord volcanic massif is largely composed of effusive rocks ranging from basalt to andesite.

CONCLUSIONS

The research reported above helped identify the structure of the Rikord volcanic massif as consisting of four volcanic edifices that coalesced at their bases; the massif is most likely of Quaternary age (Middle to Late Pleistocene, possibly the end of the Calabrian, when the Matuyama–Brunhes geomagnetic inversion occurred). The Rikord Strait was found to contain several faults, while the Rikord massif itself is situated within the nearly north–south Rikord graben.

The existence of a nearly continuous series of chemical compositions from basalt to andesite, the presence of transitional varieties from andesine to bytownite to zonal plagioclase crystals, and the gradual replacement of mafic mineral associations with sialic ones, taken together suggests the effusion of basaltic and basaltic andesite lavas during the earlier stages in the life of the Rikord volcanic massif. The melt had temperatures reaching ~1200–1300°C. As the basalts were crystallizing, the parent melt was depleted in mafic components and enriched in sialic ones. This differentiation resulted in the effusion of andesite flows.

The high values of natural remanent magnetization in dredged rocks are due to a high concentration of single-domain and pseudo-single-domain titanomagnetite and magnetite grains. The Koenigsberger ratio

Table 3. The effective magnetization J_{ef} of anomaly-inducing bodies

Body #	1	2	3	4	5	6	7	8	9	10
J_{ef}, A/m	1.4	1.7	1	1.6	1.3	1	1.7	1.3	2	1.1
Magnetization angle (deviation from the vertical) of J_{ef}, °	14	11	23	5	11	20	2	10	20	10
Maximum depth of penetration, km	6.4	10	6.6	6.4	10	10	5.4	10	10	10

for all basalt samples lies in the 1.5–16.6 range; basalt is probably the main source of the observed magnetic anomalies due to the Rikord volcanic massif.

We found a nearly vertical, a southwestern, and a south–southeastern direction for the conduits, and detected peripheral magma chambers at a depth of ~2 km.

A 3D model for the middle of the Rikord massif was developed containing ten magnetically disturbing blocks; these are most likely cooled nearly vertical magma-conducting passageways.

ACKNOWLEDGEMENTS

This work was supported by the Russian Foundation for Basic Research, project nos. 15-05-02955-a and 15-05-01823-a.

REFERENCES

Anikin, L.P., Blokh, Yu.I., Bondarenko, V.I., et al., New evidence for the structure of underwater volcanoes and islands at the Kuril Island Arc, in *Materialy XX regional'noi nauchnoi konferentsii "Vulkanizm i svyazannye s nim protsessy", posvyashchennoi Dnyu vulkanologa* (Proc. XX Regional Conference *Volcanism and Related Processes* devoted to Volcanologist's Day), March 30–31, 2017, Petropavlovsk-Kamchatskii: IViS DVO RAN, 2017, pp. 94–97.

Babayants, P.S., Blokh, Yu.I., and Trusov, A.A., Interpretation tomography based on data from gravity and magnetic surveys in the SIGMA-3D program package, in *Voprosy teorii i praktiki geologicheskoi interpretatsii gravitatsionnykh, magnitnykh I elektricheskikh polei* (Theory and Practice in the Geological Interpretation of Gravity, Magnetic, and Electrical Fields), *Materialy 31 sessii Mezhdunarodnogo seminar aim. D.G. Uspenskogo* (Proc. 31th Session of the Uspensky International Seminar), Moscow: OIFZ RAN, 2004, pp. 88–89.

Babayants, P.S., Blokh, Yu.I., Bondarenko, V.I., et al., The use of the SIGMA-3D structural interpretation program package in a study of underwater volcanoes at the Kuril Island Arc, *Vestnik KRAUNTs, Nauki o Zemle,* 2005, no. 2, Issue 6, pp. 67–76.

Bezrukov, L.P., Zenkevich, N.L., Kanaev, V.F., and Udintsev, G.B., Seamounts and volcanoes at the Kuril Island Arc, Trudy *Labor. Vulkanol.,* 1958, no. 13, pp. 71–88.

Blokh, Yu.I. and Trusov, A.A., The IGLA software for interactive interpretation of local gravity and magnetic anomalies, in *Voprosy teorii i praktiki geologicheskoi interpretatsii geofizicheskikh polei* (Theory and Practice in the Geological Interpretation of Geophysical Fields), Proc. 34th session of the Uspensky International Seminar, Moscow: IFZ RAN, 2007, pp. 36–38.

Blokh, Yu.I., Kaplun, D.V., and Konyaev, O.N., The interpretation of potential fields by methods of singular points in the SINGULAR integrated system, *Izvestiya Vuzov, Geol. Razv.,* 1993, no. 6, pp. 123–127.

Blokh, Yu.I., Bondarenko, V.I., Dolgal', A.S., et al., Advanced interpretation technologies for a multidisciplinary modeling of the Makarov underwater volcano, Kuril Island Arc, *Geoinformatika,* 2012, no. 4, pp. 8–17.

Blokh, Yu.I., Bondarenko, V.I., Dolgal', A.S., et al., Multidisciplinary studies of the Rokird massif, Kuril island arc, in *Materialy regional'noi konferentsii "Vulkanizm i svyazannye s nim protsessy", posvyashchennoi Dnyu vulkanologa* (Proc. regional conf. *Volcanism and Related Processes* devoted to Volcanologist's Day), March 29–30, 2013, academician Gordeev, E.I., Editor-in-Chief, Petropavlovsk-Kamchatskii: IViS DVO RAN, 2013, pp. 167–173.

Blokh, Yu.I., Bondarenko, V.I., Dolgal', A.S., et al., Underwater volcanism in the Sea-of-Okhotsk slope of Central Kuril Islands, in *Geologicheskie protsessy v obstanovkakh subduktsii, kollizii i skol'zheniya litosfernykh plit* (Geological Processes in Settings Involving Suduction, Collison and Sliding of Plates), Proc. Second All-Russia conf. with international participation, Vladivostok, September 17–20, 2014, Vladivostok: Dal'nauka, 2014, pp. 16–19.

Blokh, Yu.I., Rashidov, V.A., and Trusov, A.A., Estimating the remanent magnetization of submarine volcanoes at the Kuril island arc using the IGLA software, *Vestnik KRAUNTs, Nauki o Zemle,* 2015, no. 2, Issue 26, pp. 5–10.

Blokh, Yu.I., Bondarenko, V.I., Dolgal', A.S., et al., New evidence for the structure of the Rikord and Ratmanov underwater volcanic massifs, Kuril Island Arc, in *Voprosy teorii I praktiki geologicheskoi interpretatsii geofizicheskikh polei* (Theory and Practice in the Interpretation of Geophysical Fields), *Materialy 44 sessii Mezhdunarodnogo seminar im. D.G. Uspenskogo* (Proc. 44th Session of the Uspensky International Seminar), Moscow, January 23–27, 2017, Moscow: IFZ RAN, 2017, pp. 53–58.

Bondarenko, V.I., The structure of the volcanic depression in the Kraternaya Bay, Kuril Islands as inferred from seismoacoustic surveys, *Vulkanol. Seismol.,* 1986, no. 5, pp. 96–100.

Bondarenko, V.I., The structure and hypothetical evolution of the Ushishir volcanic massif, Central Kuril Islands, in *Geologiya morei i okeanov* (The Geology of Seas and Oceans), Proc. XXI International conference (school) on marine geology, vol. V, Moscow: GEOS, 2015, pp. 48–52.

Bondarenko, V.I. and Rashidov, V.A., The geomorphology and tectonics of the Middle Kuril Islands, in *Geologiya morei i okeanov* (The Geology of Seas and Oceans), Proc. XVII Intern. conf. (school) on marine geology, vol. IV, Moscow: GEOS, 2007, pp. 32–33.

Bondarenko, V.I. and Rashidov, V.A., The neotectonics of the central link in the Kuril island arc, in Fizika geosfer (The Physics of Geospheres), The seventh All-Russia symposium, September 5–9, 2011, Vladivostok: Dal'nauka, 2011a, pp. 390–393.

Bondarenko, V.I. and Rashidov, V.A., The underwater volcanoes of the Central Kuril Islands, in Vulkanizm i geodinamika (Volcanism and Geodynamics), Proc. V All-Russia symposium on volcanology and paleovolcanology, November 21–25, 2011, Yekaterinburg, Yekaterinburg: IGG UrO RAN, 2011b, pp. 404–406.

Day, R., Fuller, M., and Schmidt, V.A., Hysteresis properties of titanomagnetites: grain-size and compositional

dependence, *Physics of the Earth and Planetary Interiors,* 1977, vol. 13, pp. 260–267.

Deer, W.A., Howie, R.A., and Zussman, J., *Rock-Forming Minerals,* vol. 2, London: Longman, 1962.

Gorshkov, G.S., *Vulkanizm Kuril'skoi ostrovnoi dugi* (The Volcanism of the Kuril Island Arc), Moscow: Nauka, 1967.

Kamchatka, Kuril'skie i Komandorskie ostrova: istoriya razvitiya rel'efa (Kamchatka, Kuril and Commander Islands: A History of Relief Evolution), Moscow: Nauka, 1974.

Ishizuka, Y., Nakagawa, M., Baba, A., et al., Along-arc variations of K–Ar ages for the submarine volcanic rocks in the Kurile Islands, *Abstracts of the 7th Biennial Workshop on Japan-Kamchatka-Alaska Subduction Processes (JKSP-2011),* Petropavlovsk-Kamchatskiy, Russia, August 25–30, 2011, pp. 279.

Lelikov, E.P. and Emel'yanova, T.A., Volcanogenic units in the Sea of Okhotsk and in the Japan Sea: Comparative analysis, *Okeanologiya,* 2007, vol. 47, no. 2, pp. 294–303.

Podvodnyi vulkanizm i zonal'nost' Kuril'skoi ostrovnoi dugi (Submarine Volcanism and Zonality: The Kuril Island Arc), Academician Pushcharovskii, Yu.M., Editor-in-Chief, Moscow: Nauka, 1992.

Priroda magnitnykh anomalii i stroenie okeanicheskoi kory (The Origin of Magnetic Anomalies and the Structure of Oceanic Crust), Gorodnitskii, A.M., Editor-in-Chief, Moscow: VNIRO, 1996.

Prokop'ev, A.V., Fridovskii, V.Yu., and Gaiduk, V.V., *Razlomy (Morfologiya, geometriya i kinematika)* (Faults: Morphology, Geometry, and Kinematics), A Handbook, Parfenov, L.M., Editor-in-Chief, Yakutsk: YaF SO RAN, 2004.

Rashidov, V.A., Pilipenko, O.V., and Ladygin, V.M., A comparative analysis of magnetic properties in rocks: Five active submarine volcanoes in the western Pacific, *J. Volcanol. Seismol.,* 2014, vol. 8, no. 3, pp. 168–182.

Rashidov, V.A., Pilipenko, O.V., and Petrova, V.V., Petromagnetic and microprobe studies of rocks in the Sofu underwater volcanic cluster, Izu–Bonin island arc, Pacific Ocean, *J. Volcanol. Seismol.,* 2015, no. 3, pp. 182—196.

Rashidov, V.A., Pilipenko, O.V., and Petrova, V.V., Petromagnetic and petrographic—mineralogical studies of rocks that were dredged from submarine volcanoes in the Sea-of-Okhotsk slope of the northern Kuril island arc, *Fizika Zemli,* 2016, no. 4, pp. 84—106.

Tevelev, Al.V. and Tevelev, Ark.V., A related evolution of volcanogenic-sedimentary basins and magma chambers under near-shear tension, *Dokl. Akad. Nauk,* 1996, vol. 346, no. 5, pp. 653–655.

Translated by A. Petrosyan